Meccanica (2022) 57:1767–1781
https://doi.org/10.1007/s11012-022-01546-0

GENERAL

Electrostatic pull-in instability for tweezer architectures

G. Bianchi · A. Sorrentino · E. Radi · D. Castagnetti

Received: 6 December 2021 / Accepted: 11 June 2022 / Published online: 7 July 2022

Abstract The work investigates the static pull-in instability of electrostatically actuated tweezers with tubular electrodes. At a critical voltage, named pull-in voltage, the attraction force between the two electrodes causes the unexpected pull-in of the tubular cantilevers, which defines the limit of the elastic region of the system, especially in the case of carbon-nano tubes applications. The work aims to evaluate the lower and upper bounds of pull-in parameters of a tweezer device with the use of an accurate analytical model which allows to calculate the critical voltage and deflection values of the system. In order to assess the accuracy of the analytical model, we built a prototype and measured the critical pull-in voltage for different geometrical configurations of the device. The experimental results confirm the analytical predictions, with a maximum relative difference between the experimental and analytical values of the pull-in voltage lower than 13%.

G. Bianchi (✉) · A. Sorrentino · E. Radi · D. Castagnetti
Dipartimento di Scienze e Metodi dell'Ingegneria, Università di Modena and Reggio Emilia, Via G. Amendola 2, 42122 Reggio Emilia, Italy
e-mail: giovanni.bianchi@unimore.it

A. Sorrentino
e-mail: andrea.sorrentino@unimore.it

E. Radi
e-mail: enrico.radi@unimore.it

D. Castagnetti
e-mail: davide.castagnetti@unimore.it

Keywords Tweezers devices · Electrostatic pull-in instability · Analytical model · Tubular electrodes · Experimental validation

1 Introduction

The work focuses on the pull-in instability phenomenon of cantilever bistable electrodes for electromechanical applications. Electrostatically actuated devices are a class of smart electronic systems which are used for several industrial applications, such as sensors, actuators, storage information devices, filters and resonators [1–3]. In particular, some of these devices include carbon nano-tubes (CNTs) actuators, which are widely used in the biomechanical and medical sectors [4–6] since they can act as manipulators for nanoparticles and nanoscale objects thanks to their tiny size, ultra-low mass and high resonance frequency [7–9]. The purely elastic behaviour of these peculiar devices permits to carry huge electrical currents and to sustain high current densities, which makes CNTs a fundamental component in mechatronic applications.

Typical CNT tweezers include movable electrodes which consist of two parallel wires with tubular cross-section (i.e. the cantilevers) which are electrostatically actuated by a DC voltage difference between them [10]. The voltage difference between the electrodes causes the electrostatic attraction of the CNTs with their consequent approaching. For a

threshold voltage, namely the pull-in voltage [11], the CNTs suddenly become unstable, by attaching themselves, thus causing a short-circuit of the electrodes [12]. The pull-in instability defines the stable region of the device, that depends on the maximum controllable deflection of the nanowires, and consequently, the minimum sizes of the manipulated objects [13]. Thus, the prediction of pull-in parameters, namely the pull-in voltage and the pull-in tip deflection, is fundamental in order to estimate the equilibrium positions of the device and the geometrical dimensions of the actuated manipulators. For this reason, several numerical and semi-numerical approaches are presented in literature.

The pull-in instability of CNTs subjected to electrostatic and dispersion forces is studied by Ramezani [14] by using distributed and lumped parameter models. In order to estimate the critical pull-in characteristics in CNTs, Farrokhabadi et al. [15] proposes three different approaches: (i) a lumped parameter model, (ii) a modified Adomian decomposition model and, (iii) a numerical integration model with multipurpose commercial software. Furthermore, Farrokhabadi et al. [16] used a modified variation method and a generalized differential quadrature method (DQM) in order to estimate the pull-in parameters. The dynamic governing equation of CNT tweezers is solved using DQM and fourth order Runge–Kutta method proposed by Zare [17]. Additionally, numerical techniques using finite element analysis (FEA) and Galerkin discretization method are used to predict the critical parameters [18–21]. However, these approximated methods provide errors that become significant, especially, when the pull-in instability occurs. Then, to ensure the correct operation of these devices, a more accurate approach should be used in order to estimate the pull-in bounds, i.e. the lower and upper pull-in limits; thus, these approaches techniques supply only arbitrary estimates of the critical pull-in value. Otherwise, molecular dynamics approaches can be adopted to study CNTs pull-in behaviour: unfortunately, these methods are very time-consuming and not easily employed for large scale systems [22].

Instead, Radi et al. [23–25] propose an accurate purely analytical technique for estimating the lower and upper bounds of the static pull-in parameters by focusing on the geometrical dimensions and material properties of the actuated device. Recently, Bianchi et al. [26] exploits that method to investigate pull-in phenomena in CNT cantilever actuators with tip-charge concentration. The method proposed by Bianchi provides the analytical estimates of pull-in lower and upper bound parameters for CNT tweezers under the action of electrostatic and van der Waals (vdW) forces for different geometrical parameters of the cantilevers. The experimental characterization of these electro-mechanical models are reported in the works of Akita et al. [7], Kim et al. [9] and Chang et al. [10].

The present work aims to estimate the static pull-in lower and upper bounds of an electrostatically actuated tweezers with tubular electrodes based on CNT configuration. Firstly, the work presents a comprehensive analytical model describing the electro-mechanical behaviour of tweezer architectures. In particular, the analytical model can be described by an integral equation equivalent to the nonlinear fourth-order differential equation (ODE) governing the wires instability. The proposed method allows to estimate the critical pull-in voltage and tip deflection for different geometrical parameters of the devices resulting in a variation of the pull-in factors. Secondly, in order to assess the proposed analytical model, we designed and built a millimeter scale actuator subjected to an electrostatic actuation which is able to reproduce the peculiar pull-in instability phenomenon of actuated electrodes. The tests investigated different model configurations obtained by varying the free length of the wires and the gap between the electrodes with the aim to evaluate their effect on the pull-in voltage. The experimental results exhibit an excellent agreement with the analytical predictions, where the relative difference between the predicted and experimental pull-in voltage falls in the range from 0.83 to 13%.

2 Mathematical model

2.1 The CNT tweezers model

Figure 1 shows a schematic of a typical CNT tweezers configuration. The architecture of the device consists of two tubular cantilever electrodes of length, l, external radius, r, and wall thickness, t, which are separated by an initial gap, g.

A voltage difference applied between the two wires, namely V, generates an electrostatic attractive

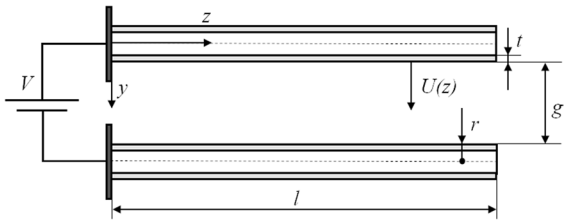

Fig. 1 Schematic of CNT tweezers under electrostatic actuation

force causing a symmetric deflection of the tubes. Specifically, *U(z)* represents the deflection of a single electrode, where z is the axial coordinate of the CNT (Fig. 1), which is the same for both the cantilevers. Usually, the system is affected by two attractive contributions: the Coulomb electrostatic force and the van der Waals intermolecular contribution, where the latter occur solely at the nano-scale, particularly when the gap, g, is lower than 20 nm.

2.1.1 Electrostatic attraction

The effect of the electrostatic force is computed by using an energetic model [27]. In particular, the wire is considered as a perfect cylindrical conductor [11, 28] with a constant voltage along its entire length. This assumption allows to use a capacitive model for the tweezer architecture [29], where the equivalent capacitance per unit length between the two cylindrical and parallel tubes, separated by the initial distance, g, is given by

$$C(g) = \frac{\pi\varepsilon_0}{\ln\left[1+\frac{g}{2r}+\sqrt{\left(1+\frac{g}{2r}\right)^2-1}\right]}, \tag{1}$$

where ε_0 is the permittivity of vacuum.

Consequently, the electrostatic energy per unit length is

$$E_e = \frac{1}{2}C(g)V^2. \tag{2}$$

Then, the attractive electrostatic force per unit length, f_e, is defined as

$$f_e = -\frac{dE_e}{dg} = \frac{\pi\varepsilon_0 V^2}{2\sqrt{g^2+4gr}\left[\ln\left(1+\frac{g}{2r}+\frac{1}{2r}\sqrt{g^2+4gr}\right)\right]^2}. \tag{3}$$

By applying an external voltage difference, i.e. V, the two electrodes deflect to each other, thus reducing the initial gap from g to $g-U_1-U_2$, where U_1 and U_2 represent the deflections of the two mobile wires, respectively. Considering that CNTs have the same geometry and material properties, the applied voltage originates the same deflection on both CNTs (i.e. $U_1 = U_2 = U$): it comes that the system is symmetric.

Then, by replacing the initial gap, g, in Eq. 3 by the effective distance $g-2U$, we obtain:

$$f_e = \frac{\pi\varepsilon_0 V^2}{2\sqrt{g^2\left(1-\frac{2U}{g}\right)\left(1-\frac{2U}{g}+\frac{4r}{g}\right)}\left[\ln\left(1+\frac{g}{2r}\left(1-\frac{2U}{g}\right)+\frac{g}{2r}\sqrt{\left(1-\frac{2U}{g}\right)\left(1-\frac{2U}{g}+\frac{4r}{g}\right)}\right)\right]^2}. \tag{4}$$

2.1.2 The van der Waals force

As reported in literature [15, 25–27], the van der Waals (vdW) interaction force can be evaluated by employing a Lennard–Jones potential model, where, the potential between atoms i and j is defined as

$$\phi_{ij} = \frac{C_{12}}{d_{ij}^{12}} - \frac{C_6}{d_{ij}^{6}}, \tag{5}$$

where d_{ij} represents the distance between two atoms, i.e. i and j, while C_{12} and C_6 represent the repulsive and attractive constants, respectively. However, for distances higher than 3.4 Å, the repulsive terms can be neglected [11] and it can be assumed $C_6 = 15.6$ eVÅ^6.

As suggested by Farrokhabadi [15] and Israelachvili [30], the van der Waals (vdW) energy can be obtained by double volume integral of the Lennard–Jones potential, that is equal to

$$E_{vdW} = \int_{v_1}\int_{v_2} n_1 n_2 \left(\frac{-C_6}{d^6(v_1, v_2)}\right) dv_1 dv_2, \tag{6}$$

where v_1 and v_2 represent the two domains of integration of CNTs, while n_1 and n_2 are the densities of atoms in these domains, and d (v_1, v_2) is the distance between any two points in these domains, i.e. v_1 and v_2.

Similarly to the equation described for the electrostatic force, i.e. Equation 3, and by considering the case of $r \ll g$ (see Fig. 1), the vdW force per unit length can be written as [15]

$$f_{vdW} = -\frac{dE_{vdW}}{dg} = -\frac{At^2}{16r^{\frac{3}{2}}(g-2U)^{\frac{5}{2}}}\left[\frac{3}{16} - \frac{5}{4}\left(\frac{r}{g-2U}\right) + \frac{35}{4}\left(\frac{r}{g-2U}\right)^2\right] \approx -\frac{3At^2}{254r^{3/2}(g-2U)^{5/2}}, \tag{7}$$

where A is the Hamaker constant [15].

2.1.3 Governing nonlinear equation of CNT configuration

From Eq. 4 and Eq. 7, the electrostatic force, f_e, and the molecular vdW force, f_{vdW}, of a CNT tweezer can be expressed as

$$f_e^*(u) = \frac{1}{\sqrt{(1-u)\left(1-u+\frac{2}{k}\right)}\left[\ln\left(1+k(1-u)+k\sqrt{(1-u)\left(1-u+\frac{2}{k}\right)}\right)\right]^2}, \tag{8}$$

$$f_{vdW}^*(u) = \frac{1}{(1-u)^{\frac{5}{2}}}, \tag{9}$$

where the dimensionless variables k, u and x are, respectively:

$$k = \frac{g}{2r},\ u = \frac{2U}{g},\ x = \frac{z}{l}. \tag{10}$$

By using a minimum energy principle [31], the governing equation of CNTs can be described through the following fourth-order nonlinear ODE

$$u^{IV}(x) = f(u(x)), \quad \text{for } 0 \le x \le 1, \tag{11}$$

and the boundary conditions for the cantilever tweezers

$$u(0) = 0, \quad u'(0) = 0, \quad u''(1) = 0, \quad u'''(1) = 0, \tag{12}$$

where the load function governing the system, namely $f(u)$, can be expressed as

$$f(u) = \beta f_e^*(u) + \alpha f_{vdW}^*(u), \tag{13}$$

where the dimensionless parameters, β and α, are proportional to the magnitude of the electrostatic force and vdW interactions, respectively, namely

$$\beta = \frac{\varepsilon_0 \pi V^2 l^4}{EIg^2}, \tag{14}$$

$$\alpha = \frac{3At^2 l^4}{256 r^{3/2} EIg^{7/2}}, \tag{15}$$

where I is the moment of inertia of the beam cross-section, defined as $I \approx \pi t r^3$ [32], t is the CNT wall thickness, ranging from 0.7 up to 3.4 Å, while E is the Young's modulus of the graphene which varies from 0.5 up to 5.5 TPa. However, for the present investigations the mean values considered are $t = 1.34$ Å and $E = 2.52$ TPa [32].

2.2 Analytical method

In order to estimate the lower and upper bounds of the pull-in voltage and tip deflection of CNTs, we propose an accurate analytical approach, similar to that developed in the works of Bianchi et al. [26] and Radi et al. [23, 24].

2.2.1 Nonlinear integral equation

Following the approaches reported in [23], the Boundary Value Problem (BVP) is equivalent to a nonlinear integral equation that is obtained exploiting the Green's function of the differential problem of Eqs. 11 and 12. In particular, by imposing the boundary conditions of cantilever beam and the continuity conditions, the coefficients of the general solution to this problem can be univocally determined

$$G(t) = \begin{cases} \frac{t^2(3x-t)}{6}, & 0 \le t < x, \\ \frac{x^2(3t-x)}{6}, & x < t \le 1. \end{cases} \tag{16}$$

Thus, the BVP of Eqs. 11 and 12 can be equivalently formulated in term of the following non-linear integral equation

$$u(x) = \frac{1}{6}\int_0^x \left[t^2(3x-t)\right] f(u(t))dt + \frac{1}{6}\int_x^1 \left[x^2(3t-x)\right] f(u(t))dt. \tag{17}$$

From Eq. 17, the maximum deflection at the tip of the cantilever ($x = 1$) is equal to

$$\delta = u(1) = \frac{1}{6}\int_0^1 t^2(3-t) f(u(t))dt. \tag{18}$$

Given that the load function of the system (i.e. $f(u)$ in Eq. 13), and its first derivative with respect to the displacement, u, (i.e. $f'(u)$), are positive and monotonically increasing, the following inequalities then hold true

$$0 \le f(0) \le f(u) \le f(\delta), \quad 0 \le f'(0) \le f'(u) \le f'(\delta) \quad \text{for } 0 \le u \le \delta. \tag{19}$$

As reported in the work of Radi [23], the inequalities in Eq. 19 provide useful properties of the function $u(x)$, that is the solution of the above mentioned BVP (see Eqs. 11 and 12).

Specifically, the function u is positive, monotonically increasing and convex, and can be used to obtain accurate lower and upper bounds estimates of the deflection of CNT tweezers, namely

$$u(x) \ge 0, \quad u'(x) \ge 0, \quad u''(x) \ge 0, \quad \text{for } x \in [0, 1]. \tag{20}$$

2.2.2 Upper and lower bounds for the deflection

In order to define the upper and lower bounds of the critical pull-in parameters, two-side estimates are first derived for the deflection $u(x)$. As reported in Radi et al. [23], $u(x)$ denotes the solution to the ODE of Eq. 11 that satisfy the boundary conditions of Eq. 12, then

$$u(x) \le u_U(x), \quad \text{for } x \in [0, 1] \tag{21}$$

where $u_U(x)$ is the upper bound of the deflection $u(x)$, then yields

$$u_U(x) = \delta \cdot b(x), \tag{22}$$

where $b(x)$ is obtained from [23] and defined as

$$b(x) = \frac{1}{3}\left(6x^2 - 4x^3 + x^4\right) \tag{23}$$

Similarly, the lower bound of the deflection (see Ref [23].), namely $u_L(x)$, can be obtained as

$$u(x) \ge u_L(x) \quad \text{for} x \in [0, 1] \tag{24}$$

$$u_L(x) = \delta \cdot a_1(x) + f(0) \cdot a_2(x), \tag{25}$$

where

$$\begin{aligned} a_1(x) &= (3x^2 - x^3), \\ a_2(x) &= (3x^2 - 5x^3 + 2x^4). \end{aligned} \tag{26}$$

And the load function, $f(u)$, computed in $u=0$ is defined as

$$f(0) = \frac{\beta}{\sqrt{1+\frac{2}{k}}\left[\ln\left(1+k+k\sqrt{1+\frac{2}{k}}\right)\right]^2} + \alpha, \tag{27}$$

where $b(x)$, $a_1(x)$ and $a_2(x)$ in Eqs. 23 and 26 represent the polynomials that define the limits of the deflection [23]. Specifically, upper and lower bounds in Eqs. 22 and 25 are obtained by the boundary conditions in Eq. 12. For this reason, these polynomials are the same reported in [23], with a different f (0) since the load functions affecting the two devices are different.

2.2.3 *Upper and lower bounds for the pull-in parameters*

By introducing the upper and lower estimates Eqs. 22 and 25 in Eq. 18 for the normalized CNTs tip deflection, the lower and upper bounds for the pull-in parameters can be derived.

2.2.3.1 Lower bounds to the pull-in parameters By using Eqs. 18 and 21 it follows

$$\delta \le \frac{1}{6}\,[\beta\, L(\delta) + F(\delta)], \tag{28}$$

where the functions $L(\delta)$ and $F(\delta)$ are defined as

$$L(\delta) = \int_0^1 \frac{t^2(3-t)}{\sqrt{(1-\delta\, b(t))\left(1-\delta\, b(t)+\frac{2}{k}\right)}\left[\ln\left(1+k-k\,\delta\, b(t)+k\sqrt{(1-\delta\, b(t))\left(1-\delta\, b(t)+\frac{2}{k}\right)}\right)\right]^2}\, dt, \tag{29}$$

$$F(\delta) = \alpha \int_0^1 \frac{t^2(3-t)}{[1-\delta\, b(t)]^{5/2}}\, dt,$$

where $L(\delta)$ and $F(\delta)$ can be evaluated numerically. Specifically, Eq. 28 defines a lower bound for the relation between the electrostatic loading parameter, β, and the normalized pull-in deflection, δ. The maximum value of β, and the corresponding tip deflection, δ, are obtained from Eq. 28, using the stationary condition

$$\frac{\partial \beta}{\partial \delta} = 0. \tag{30}$$

Then, it is possible to define the lower bounds of pull-in parameters, namely β_L and δ_L, such that

$$\begin{aligned} \beta_{PI} &\ge \beta_L, \\ \delta_{PI} &\ge \delta_L, \end{aligned} \tag{31}$$

where β_{PI} and δ_{PI} represent the exact solution of the BVP problem of Eqs. 11 and 12, for the pull-in instability of the CNT tweezers.

The analytical lower bounds, i.e. β_L and δ_L, are obtained by the following two conditions

$$\begin{aligned} \beta_L L(\delta_L) + F(\delta_L) &= 6\delta_L, \\ \beta_L L'(\delta_L) + F'(\delta_L) &= 6, \end{aligned} \tag{32}$$

where the functions $L'(\delta_L)$ and $F'(\delta_L)$ represent the first derivative with respect to δ of the functions $L(\delta)$ and $F(\delta)$ in Eq. 29, and can be estimated numerically.

2.2.3.2 Upper bounds to the pull-in parameters By using Eqs. 18 and 24 it follows

$$\delta \ge \frac{1}{6}\,[\beta\, K(\delta,\ \beta) + H(\delta,\ \beta)], \tag{33}$$

where the functions $K(\delta,\beta)$ and $H(\delta,\beta)$ are defined as

$$K(\delta,\beta) = \int_0^1 \frac{t^2(3-t)}{\sqrt{\left(1-\left[\delta\, a_1(t)+f(0)a_2(t)\right]\right)\left(1-\left[\delta\, a_1(t)+f(0)a_2(t)\right]+\frac{2}{k}\right)}}\cdot$$
$$\cdot\frac{1}{\left[\ln\left(1+k-k\left[\delta\, a_1(t)+f(0)a_2(t)\right]+k\sqrt{\left(1-\left[\delta a_1(t)+f(0)a_2(t)\right]\right)\left(1-\left[\delta\, a_1(t)+f(0)a_2(t)\right]+\frac{2}{k}\right)}\right)\right]^2}\,dt,$$
$$H(\delta,\beta)=\alpha\int_0^1 \frac{t^2(3-t)}{\left(1-\left[\delta\, a_1(t)+f(0)a_2(t)\right]\right)^{5/2}}\,dt, \tag{34}$$

where $K(\delta,\beta)$ and $H(\delta,\beta)$ can be evaluated numerically.

Specifically, Eq. 33 defines an upper bound to the relation between the parameters β and δ.

The maximum value of β, and the corresponding tip deflection, δ, obtained by using the stationary condition (see Eq. 28), provides the upper bounds of the pull-in parameters, namely β_U and δ_U, such that

$$\begin{aligned}\beta_{PI} &\le \beta_U,\\ \delta_{PI} &\le \delta_U.\end{aligned} \tag{35}$$

Then, the upper bounds follow from the following two conditions

$$\begin{aligned}\beta_U K(\delta_U,\beta_U)+H(\delta_U,\beta_U)&=6\delta_U,\\ \beta_U K'(\delta_U,\beta_U)+H'(\delta_U,\beta_U)&=6,\end{aligned} \tag{36}$$

where the functions $K'(\delta_U,\beta_U)$ and $H'(\delta_U,\beta_U)$ represent the first derivative with respect to δ of the functions $K(\delta,\beta)$ and $H(\delta,\beta)$ in Eq. 34, and can be estimated numerically.

2.2.4 *The approximated pull-in voltage in tweezer devices with negligible intermolecular interactions*

As shown in Eqs. 13–15, α and β remarkably affect the values of critical pull-in parameters, and consequently, the operation point of the nanowires. However, when the geometrical dimensions of the tweezers increase, the contribution of the intermolecular vdW forces decrease (i.e. $\alpha=0$). Specifically, if the gap between the CNTs increases from the nano- to micro-scale, then the intermolecular force becomes negligible. In this specific operating condition, only the electrostatic force determines the pull-instability threshold of the tweezers.

Thus, by solving the BVP of the pull-in instability introduced in Eqs. 11 and 12, the parameter β takes the following expression

$$\beta^* = \frac{61.1070+28.2748k+0.129635k^2}{12.2183+0.469347k+0.000679689k^2}, \tag{37}$$

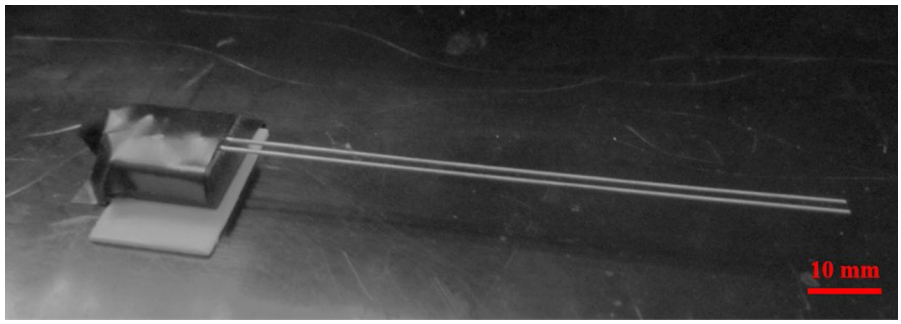

Fig. 2 Macro-scale device implemented

where the geometrical parameter k is defined as in Eq. 10, and the numerical coefficients are obtained by interpolation of the analytical upper and lower estimates using the *Mathematica* software [33].

Then, from Eq. 14, the value of the critical pull-in voltage of the CNTs device, namely V_{PI}^{*}, can be expressed as

$$V_{PI}^{*} = \sqrt{\beta^{*}\frac{EIg^{2}}{\varepsilon_{0}\pi l^{4}}}, \tag{38}$$

where the geometrical and material parameters are the same reported as in Sect. 2.1.3.

3 Experimental characterization of macro-scale tweezers

The experimental validation focused on the electrostatically actuated model in Sect. 2.2.4, which represents the typical operating condition in most of cantilever actuators, given that the electrostatic input constitutes the principal attractive contribution in CNT architecture.

3.1 Prototype development

The switching configuration examined is the same described in Fig. 1, with the only exception that we considered a solid cylinder, since the value of the parameter β in Eq. 14 is not affected by the thickness, t, of the wire.

As shown in previous works from literature [34–38], to simplify the experimental approach, the experimental characterization focused on a macro-scale model of the CNT configuration. Specifically, by keeping constant the ratio between the geometrical dimensions of the system, it is possible to obtain a macro-scale model of the tweezers by increasing the geometrical dimensions of the nano-system. The macro-scale size system obtained is able to reproduce the static pull-in phenomena of electrostatically actuated tweezer configuration, where the intermolecular forces are negligible (see Sect. 2.2.4).

As shown in Fig. 2, the switching system is composed by two suspended wires made of steel C100 with constant radius, r, equal to 0.225 mm, and with a free length, l. The wires are separated by an initial gap, g, and clamped at one end to a 3D printed ABS support that acts as a dielectric between the flexible wires. For the wires we assumed a Young's modulus, E, equal to 210 *GPa*, and a Poisson's ratio, $v = 0.3$. Moreover, the system is subject to an electrostatic actuation, namely V_{out}.

Table 1 Average values of real dimension for the different specimens tested

Specimen	r [mm]	l [mm]	g [mm]	k
1	0.225	73.00 ± 0.05^{a}	0.81 ± 0.05^{a}	1.80
2	0.225	70.00 ± 0.05^{a}	0.82 ± 0.05^{a}	1.82
3	0.225	56.50 ± 0.05^{a}	0.59 ± 0.05^{a}	1.31
4	0.225	56.40 ± 0.05^{a}	0.66 ± 0.05^{a}	1.47
5	0.225	65.70 ± 0.05^{a}	0.84 ± 0.05^{a}	1.87
6	0.225	74.40 ± 0.05^{a}	0.78 ± 0.05^{a}	1.73

[a]((mean ± standard deviation))

Due to the macro scale, the device required a high actuation voltage to reach the pull-in threshold. For this reason, we used a high voltage DC–DC converter (*EMCO CB101*) that provides an output voltage, i.e. V_{out}, in a range between 0 and ± 10 kV. The high voltage DC-DC converter is powered by a 12 V power supply and controlled by a simple electric circuit that allows to regulate the output voltage. Specifically, the regulation circuit consists of a voltage divider and of a manual multi-turn potentiometer that allows to regulate the output voltage (i.e.V_{out}) from the DC–DC converter, from 0 up to the pull-in threshold, i.e.V_{PI}. Thus, the critical value of the output voltage corresponds to the critical pull-in voltage, V_{PI}.

Consequently, the high voltage output pin of the DC–DC converter was connected to the clamped end of the suspended electrodes where the wires are bonded. These electric circuit and the voltage system regulation are the same described in [35]. Since the critical pull-in voltage is affected by the geometric dimensions of the wires and by the initial gap between them [35], we set the maximum admissible pull-in voltage equal to 3000 V, thus avoiding unexpected breakdown phenomena.

3.2 Experimental validation

3.2.1 Experimental set-up

The experimental validation aims to measure the critical pull-in voltage of the actuated tweezers of the

Table 2 Values of lower and upper pull-in parameters of a CNT tweezers, for different values of the parameter α and the geometric ratio k

α	$k=10$				$k=100$				$k=1000$			
	δ_L	β_L	δ_U	β_U	δ_L	β_L	δ_U	β_U	δ_L	β_L	δ_U	β_U
0.0	0.5196	21.542	0.5286	21.855	0.5471	63.000	0.5562	63.886	0.5726	135.76	0.5817	137.63
0.3	0.4793	16.568	0.4887	16.946	0.4961	48.040	0.5054	49.035	0.5103	102.59	0.5196	104.64
0.6	0.4471	11.824	0.4573	12.299	0.4574	34.074	0.4670	35.150	0.4658	72.330	0.4753	74.484
1.0	0.4114	5.7578	0.4229	6.4018	0.4158	16.487	0.4257	17.631	0.4192	34.796	0.4290	36.956
1.2	0.3957	2.8126	0.4079	3.5572	0.3976	8.0320	0.4078	9.1947	0.3993	16.913	0.4091	19.026
1.4	0.3810	−0.083	0.3940	0.7720	0.3809	−0.236	0.3913	0.9337	0.3809	−0.497	0.3909	1.5371

macro-scale model in Sect. 2.2.4. In particular, we supplied the device with a power supply up to reach the pull-in threshold, and regulated the input voltage to the DC–DC converter using the multi-turn potentiometer (see Sect. 3.1).

During the test, a National Instrument acquisition board (NI 9211) measured the pull-in voltage on the device until the system reached the pull-in. The acquisition board was connected to a notebook that registered and processed the acquired data using an algorithm implemented in LabVIEW [39]. For further details of the experimental benchmark see Ref. [35].

3.2.2 Test plan

In order to assess the analytical model in Sect. 2.2.4, we investigated some different configurations of the tweezers to examine the influence of the geometrical parameters on the pull-in.

Table 1 reports the average values of the six tweezers configurations investigated experimentally, where k is the same described in Eq. 10.

Specifically, we tested different specimen configurations which have different free length, l, in combination of different gaps between the wires, g, and where the external radius of the wire, r, is fixed to 0.225 mm (Fig. 1). Thus, for all the six configurations in Table 1, we performed 5 replications of the pull-in tests, for a total of 30 tests. In particular, the real geometrical dimensions of the system were obtained by image processing using Image J software [40], thus obtaining an accurate estimate of the geometrical parameters of the switching system.

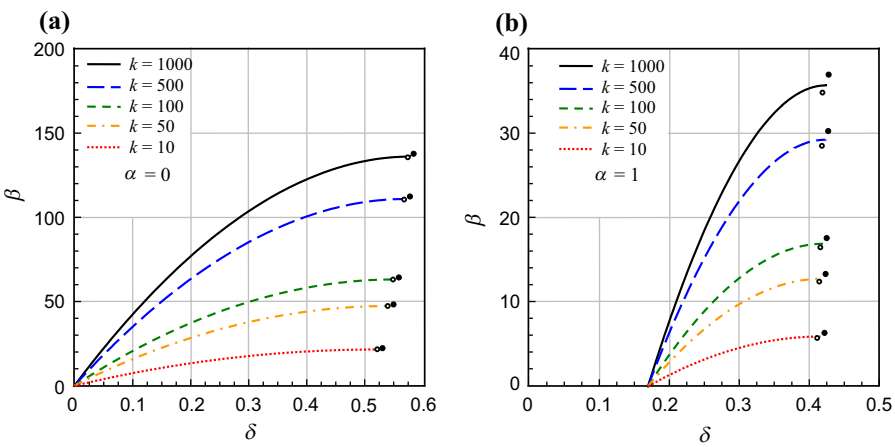

Fig. 3 Variations of the tip deflection parameter δ with the pull-in parameters β obtained from the shooting method, for various values of the geometric parameter k and for the vdW force parameter $\alpha=0$ (**a**) and $\alpha=1$ (**b**). The curves display the numerical solutions, while the lower and upper analytical values of the pull-in parameters, i.e.β_L and β_U, are indicated by empty circles and solid circles, respectively

4 Results and discussion

4.1 Analytical estimates

Table 2 reports the analytical predictions of the lower and upper bounds for the dimensionless pull-in voltage parameter, i.e. β_L and β_U, and the corresponding values of the dimensionless pull-in deflection parameter, δ_L and δ_U, for different values of the van der Waals force parameter, α, and three levels of the dimensionless parameter k, from 10 to 1000 (see Eq. 10). It is worth noting that the value of the parameter k is usually greater than 80, which correspond to a tweezer of radius, r, of 5 nm, with a value of the gap between the electrodes, g, equal to 800 nm [7, 9].

From Table 2 it can be observed that the pull-in voltage and deflection parameters significantly decrease by increasing the contribution of vdW force parameter, α. These results suggest that the pull-in voltage and deflection significantly decrease if the contribution of the vdW force is considered, namely as the coefficient α increases. Otherwise, the pull-in parameters increase as the geometric ratio k increases. These predictions confirm the well-known effect of the vdW parameter α and the geometric ratio k. However, if the gap, g, is typically above 20 nm, the contribution of the vdW forces can be neglected, especially for the case of metal wires.

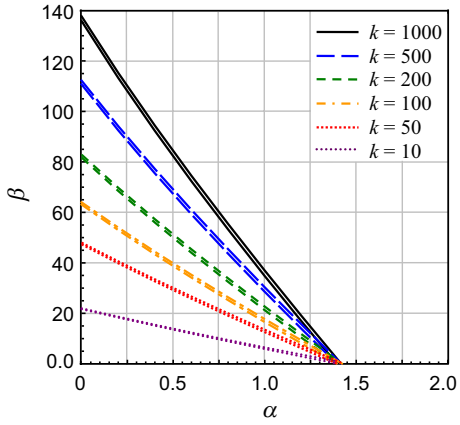

Fig. 5 Influence of the van der Waals force parameter, α, on the pull-in parameter β, for different values of geometric ratio k. For each value of the ratio k, the top curve corresponds to the upper estimate while the bottom curve to the lower estimate for β

Moreover, if the vdW force parameter α is greater than its critical value, ranging between 1.3942 and 1.4229, a repulsive electrostatic force with negative value is required to prevent pull-in instability and the consequent occurrence of stiction of tweezers (see last row in Table 2).

Figure 3 shows the relation between the pull-in voltage parameter, β, and the tip deflection parameter of the tweezer, δ, for different values of parameter k:

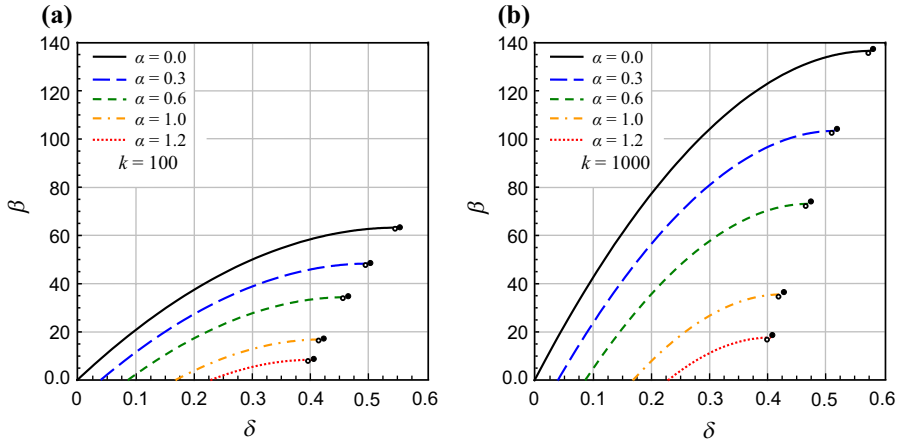

Fig. 4 Variations of the tip displacement parameter δ with the pull-in voltage parameters β obtained from the shooting method, for various values of the vdW parameter α and for the geometric coefficient $k = 100$ (**a**) and $k = 1000$ (**b**). The curves display the numerical solutions, while the lower and upper analytical values of the pull-in parameters, i.e. β_L and β_U, are indicated by empty circles and solid circles, respectively

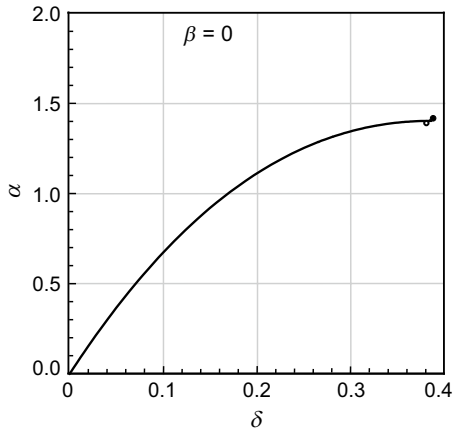

Fig. 6 Relationships between vdW parameter α and tip deflection parameter δ obtained from the shooting method, for a free-standing CNT tweezers ($\beta=0$). Lower and upper estimates of the pull-in parameters are indicated by empty circles and solid circles, respectively

the case of $\alpha=0$ is considered in Fig. 3.a, while the case of $\alpha=1$ is considered in Fig. 3.b. Specifically, the lower and upper analytical estimates of the pull-in parameter, i.e.β_L and β_U, calculated by using the accurate method described in Sect. 2.2, are marked with empty circles and solid circles, respectively. In order to validate the analytical estimates, a numerical integration approach based on the shooting method available in *Mathematica*® [33] is employed for obtaining a numerical solution of the boundary value problem (BVP) defined by the nonlinear ODE and the boundary conditions in Sect. 2.1.3. In particular, the curves in Fig. 3 display the variation of dimensionless CNT pull-in voltage obtained from the shooting method, for various values of the geometric ratio k.

As depicted in Fig. 3, the pull-in voltage parameter β increases, by increasing the value of the coefficient k. Conversely, the increase of the vdW coefficient (i.e. α) yields a significant decrease of the pull-in voltage parameters β and δ. The analytical pull-in bounds, i.e. β and δ, are in good agreement to the numerical pull-in parameters obtained by the shooting method, i.e. β_{PI} and δ_{PI}, confirming the accuracy of the proposed

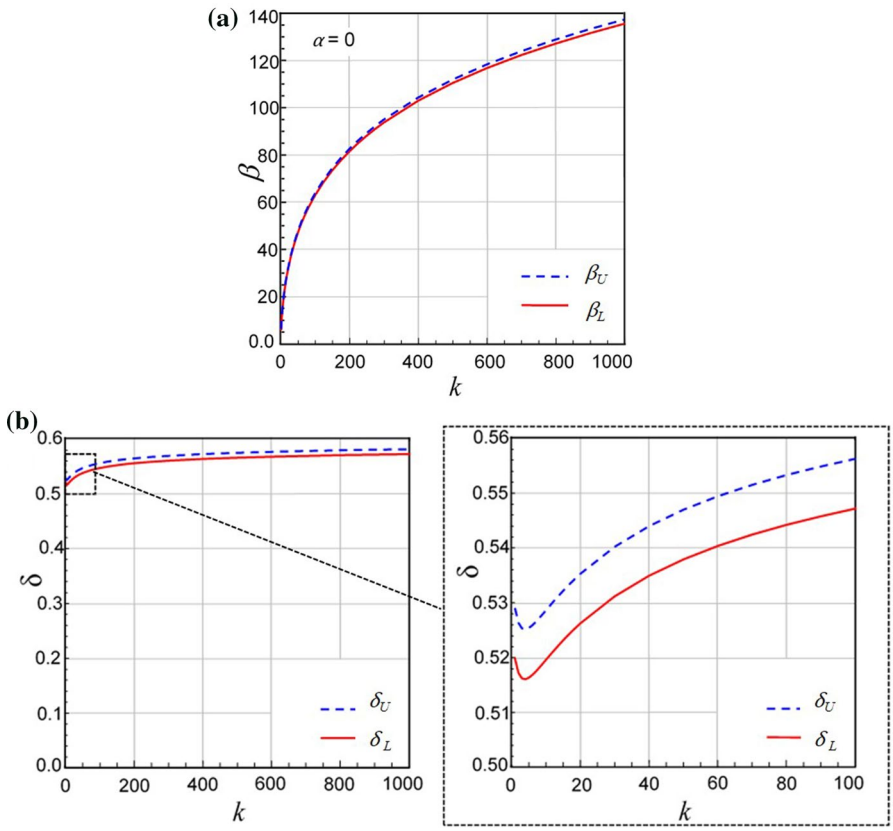

Fig. 7 Variations of β_L and β_U (**a**) and δ_L and δ_U (**b**) with respect to k according to Eq. 32 and Eq. 36 for a CNT tweezers, for the case of $\alpha=0$

method (see Fig. 3). On the one hand, for the case of $\alpha=0$, the maximum relative error between the analytical and numerical estimates of the pull-in voltage parameter, β, and of the pull-in deflection parameter, β, is lower than 0.75% and 0.88%, respectively (i.e. $k=1000$ in Fig. 3a). On other hand, for $\alpha=1$, the maximum relative difference is lower than 3.86% for the pull-in voltage parameter, β, and lower than 1.27% for the pull-in deflection parameter, δ (i.e. $k=1000$ in Fig. 3b).

Similarly, Fig. 4 reports the effect of vdW force contribution, i.e. α, on the pull-in parameters β and δ, by considering two values of the geometric ratio, k, equal to 100 (see Fig. 4a) and 1000 (see Fig. 4.b). We highlighted that, the high values of k strongly affect the pull-in response of the CNTs, since the initial gap between the nanotubes is typically much greater than the diameter of tubular electrodes. However, larger values of pull-in parameters are obtained neglecting vdW paraemeter, $\alpha=0$, and for higher geometric coefficients k (e.g. black line in Fig. 4b). Moreover, the results plotted in Fig. 4 reveal that the CNT tweezers are initially deflected due to the presence of vdW force even when no electric voltage is applied, namely for $\beta=0$: this phenomenon is called freestanding of the nanowires. As observed in Fig. 3, the increase of α, and the corresponding increase of the parameter k up to 1000, leads to increase the relative error between the numerical and analytical estimates: which is nearly equal to 7.76% for the dimensionless pull-in voltage, β, and of 1.38% for the pull-in deflection parameter, δ (i.e. red line in Fig. 4b).

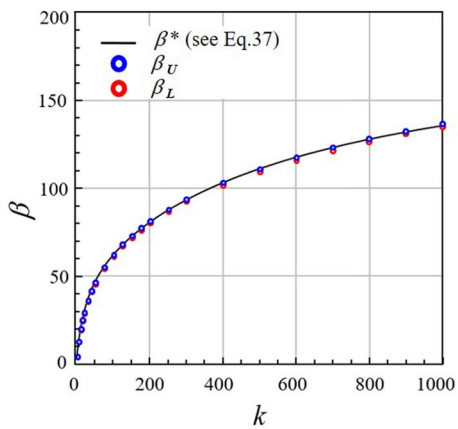

Fig. 8 Variation of pull-in parameter β with respect to k for an electrostatically actuated CNT system with $\alpha=0$ (see Sect. 2.2.4). The curve displays the numerical solution, while the lower and upper estimates of the pull-in load factor are indicated by empty circles

Table 3 Comparison between the experimental and approximated pull-in voltage, namely V_{PI}^{E} and V_{PI}^{*}, where the corresponding approximated value of the dimensionless pull-in voltage, β^{*}, is obtained by using Eq. 37

Specimen	V_{PI}^{E}[V]	V_{PI}^{*}[V]	Error [%]
1	1860 ± 67^{a}	1738	6.56
2	1934 ± 20^{a}	1918	0.83
3	2060 ± 47^{a}	1995	3.15
4	2320 ± 91^{a}	2283	1.59
5	2400 ± 87^{a}	2241	6.62
6	1940 ± 75^{a}	1600	13.04

[a] (Mean ± standard deviation)

Figure 5 shows the variations of dimensionless upper and lower pull-in voltage, β_U and β_L, with vdW parameter, α, for different values of the geometric ratio parameter k. In particular, the curves in Fig. 5 were obtained by interpolating the analytical estimates of lower and upper pull-in voltage. These results show that the lower and upper analytical bounds are very close each other for every value of the coefficients α and geometric ratio k. As depicted in Fig. 5, when no electric voltage is applied to the system (i.e. $\beta=0$), we can observe the freestanding CNT tweezers phenomenon: specifically, all the curves obtained for different geometric coefficient k have the same lower and upper critical values of vdW force parameter, $\alpha_L=1.3942$ and $\alpha_U=1.4229$. Specifically, Fig. 6 compares the analytical and numerical results for the critical vdW force coefficient, α,

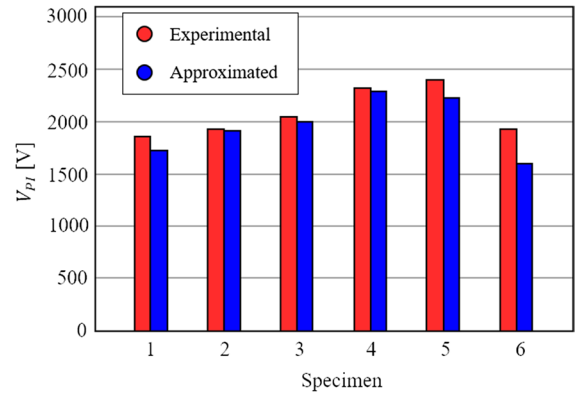

Fig. 9 The experimental and approximated pull-in voltage variation for the different cases evaluated in Table 1

with the corresponding tip deflection parameter, δ, for a freestanding CNT tweezers ($\beta=0$), which is independent of the value of k. Thus, the maximum relative error between the analytical and numerical estimates of the vdW parameter, α, and of the pull-in deflection coefficient, δ, is lower than 1.5% and 1.3%, respectively.

Figure 7 reports the effect of the parameter k on the lower and upper bounds for the pull-in voltage coefficient β_{PI} (see Fig. 7.a), and the corresponding tip deflection parameter δ_{PI} (see Fig. 7b), by neglecting the vdW parameter ($\alpha=0$). These outcomes confirm the behaviour of pull-in parameters (i.e. β_{PI} and δ_{PI}), for the different value of k, which can be observed in Fig. 3 and Fig. 4. In particular, for very small values of geometric ratio, namely $k<5$, it can be observed a brief decreasing phase of pull-in deflection coefficient δ_{PI} (see Fig. 7b). However, for high values of k, namely for gap much larger than the diameter of the tubes, the pull-in deflection is almost unaffected by further variation of the parameter k. Additionally, Fig. 7 shows that the lower and upper analytical bounds are very close each other, regardless the value of the coefficient k: moreover, the larger distance observed in Fig. 7.b is due to the scale of the graph, thus the accuracy of the provided analytical approach is confirmed.

Figure 8 presents the variation of the pull-in parameter β with respect to k, for the specific case of an electrostatically actuated CNT tweezers, namely for the case of $\alpha=0$ (see Sect. 2.2.4), where the analytical estimates are obtained using Eq. 37. The approximated curve, obtained with *Mathematica*®, fits very well the lower and upper estimates of the dimensionless pull-in voltage parameter, β, thus ensuring the accuracy of Eq. 37.

In particular, the increase of the value of k, improved the accuracy of the approximated estimates with respect to the analytical ones, especially for CNT tweezers, where $g>>r$ [15].

4.2 Experimental results of macro-scale configuration

Table 3 compares the critical pull-in voltage for the six configurations investigated (see Table 1) where, V_{PI}^{E} represents the experimental pull-in voltage and V_{PI}^{*}, the approximated pull-in voltage obtained using Eq. 38. In particular, for the experimental values of the pull-in voltage, we reported the mean value and the corresponding standard deviation for the 5 replications performed. The experimental results in Table 3 exhibit an excellent agreement with the analytical prediction. In particular, relative difference between the experimental measurements and the approximated values of the pull-in voltage falls in the range between 0.83% and 13.04%.

As shown in Fig. 9, it appears that both the free length, l, and the value of the initial gap, g, of the system affected the amount of the pull-in voltage. Specifically, the higher the length of the tweezer, l, the lower the value of the pull-in voltage. However, by decreasing the value of the gap, g, the pull-in voltage decreases, according to Eq. 38.

Moreover, the scatter in the value of the pull-in voltage, can be imputed to the following issues. First, the combined effect of the inaccuracies in the gap (i.e. g) and in the free length (i.e. l) of the experimental device. In particular, a 0.05 mm variation in the gap, g, can lead a scatter of the pull-in voltage between 125 and 150 V. Second, additional inaccuracies are determined by a not perfect alignment of the two electrodes, resulting in a variation of the initial gap, g. It is worth noting that for specimens 4 and 5, were registered critical pull-in voltages close to the maximum admissible pull-in voltage of the device, that is lower than 2500 V.

Nevertheless, the proposed macro-scale specimen is a low-cost solution with the only limitation of high actuation voltage to reach the pull-in phenomenon, as highlighted in Table 3.

However, the macro-scale prototype implemented is able to reproduce the same pull-in phenomenon observed in the micro-nano scale, with exception of the vdW surface forces. The proposed device is adaptable and simple to manufacture.

5 Conclusions

This work aimed to identify the critical pull-in parameters of cantilever bistable electrodes for nano-electromechanical tweezer applications, exploiting the smart properties of carbon nano-tubes (CNTs). The work presents a detailed electro-mechanical model of electrostatically actuated CNT tweezers under the attraction of van der Waals (vdW) forces.

In particular, we implemented an accurate analytical model of the switching system under electrostatic actuation, and used this model to derive a simple approximated formula of pull-in voltage. The analytical lower and upper bounds of critical pull-in voltage and tip deflection match very well the numerical solutions. Moreover, in order validate the approximated analytical prediction, we designed and built an electrostatically actuated macro-scale tweezer, which reproduces the same pull-in instability phenomenon of tweezer configuration. The tests investigated different macro-model configurations by varying the free length of the wires and the gap between the electrodes. The experimental results show a close agreement with the analytical predictions of the approximated method, where the maximum relative difference of the pull-in voltage is lower than 13%.

Funding This research has been performed within the framework of the grant MIUR-PRIN 2020F3NCPX "Mathematics for industry 4.0 (Math4I4)".

Declarations

Conflict of interest The author(s) declared no potential conflicts of interest with respect to the research, authorship, and/or publication of this article.

References

1. Ionescu AM (2014) Nano-electro-mechanical (NEM) memory devices. Emerging Nanoelectronic Devices, John Wiley & Sons Ltd, pp 123-136
2. Loh OY, Espinosa HD (2012) Nanoelectromechanical contact switches. Nat Nanotechnol 7:283–295
3. Spaggiari A, Castagnetti D, Golinelli N et al (2016) (2016) Smart materials: properties, design and mechatronic applications. Proc Inst Mech Eng Part L J Mater Design Appl 233:734–762
4. Göpel W (1993) Nanosystems: Molecular machinery, manufacturing and computation. By K. Eric Drexler, J. Wiley & Sons, Chichester, UK 1992, 556 pp., hardcover, £ 19.50, ISBN 0-471-57547-X. Adv Mater 5:865–866
5. Kumemura M, Collard D, Yoshizawa S, et al. (2010) Direct bio-mechanical sensing of enzymatic reaction On DNA by silicon nanotweezers. In: 2010 IEEE 23rd International Conference on Micro Electro Mechanical Systems (MEMS). pp. 915–918
6. Sounart TL, Michalske TA, Zavadil KR (2005) Frequency-dependent electrostatic actuation in microfluidic MEMS. J Microelectromech Syst 14:125–133
7. Akita S, Nakayama Y, Mizooka S et al (2001) Nanotweezers consisting of carbon nanotubes operating in an atomic force microscope. Appl Phys Lett 79:1691–1693
8. Bogue R (2009) Nanosensors: a review of recent research. Sens Rev 29:310–315
9. Kim P, Lieber CM (1999) Nanotube nanotweezers. Science 286:2148–2150
10. Chang J, Min BK, Kim J et al (2009) Electrostatically actuated carbon nanowire nanotweezers. Smart Mater Struct 18:065017
11. Dequesnes M, Rotkin SV, Aluru NR (2002) Calculation of pull-in voltages for carbon-nanotube-based nanoelectromechanical switches. Nanotechnology 13:120–131
12. Wang GW, Zhang Y, Zhao YP et al (2004) Pull-in instability study of carbon nanotube tweezers under the influence of van der Waals forces. J Micromech Microeng 14:1119–1125
13. Ke CH, Pugno N, Peng B et al (2005) Experiments and modeling of carbon nanotube-based NEMS devices. J Mech Phys Solids 53:1314–1333
14. Ramezani A (2011) Stability analysis of electrostatic nanotweezers. Physica E-low-Dimens Syst Nanostruct - PHYSICA E 43:1783–1791
15. Farrokhabadi A, Rach R, Abadyan M (2013) Modeling the static response and pull-in instability of CNT nanotweezers under the Coulomb and van der Waals attractions. Phys E 53:137–145
16. Farrokhabadi A, Mokhtari J, Koochi A et al (2015) A theoretical model for investigating the effect of vacuum fluctuations on the electromechanical stability of nanotweezers. Indian J Phys 89:599–609
17. Zare J, Shateri A (2017) Instability threshold of rippled carbon nanotube nanotweezers in the low vacuum gas flow incorporating Dirichlet and Neumann modes of Casimir energy. Phys E 90:67–75
18. Mukherjee B, Sen S (2018) Generalized closed form solutions for feasible dimension limit and pull-in characteristics of nanocantilever under the Influences of van der Waals and Casimir forces. Mater Res Exp. https://doi.org/10.1088/2053-1591/aabb8b
19. Bornassi S, Haddadpour H (2017) Nonlocal vibration and pull-in instability analysis of electrostatic carbon-nanotube based NEMS devices. Sens Actuators, A 266:185–196
20. Sedighi HM, Farjam N (2017) A modified model for dynamic instability of CNT based actuators by considering rippling deformation, tip-charge concentration and Casimir attraction. Microsyst Technol 23:2175–2191
21. Mobki H, Rezazadeh G, Vefaghi A et al (2019) Investigation of nonlinear dynamic behavior of a capacitive carbon nano-tube based electromechanical switch considering van der Waals force. Microsyst Technol 25:461–475
22. Fakhrabadi MMS, Khorasani PK, Rastgoo A et al (2013) Molecular dynamics simulation of pull-in phenomena in carbon nanotubes with Stone-Wales defects. Solid State Commun 157:38–44
23. Radi E, Bianchi G, di Ruvo L (2017) Upper and lower bounds for the pull-in parameters of a micro- or nanocantilever on a flexible support. Int J Non-Linear Mech 92:176–186

24. Radi E, Bianchi G, di Ruvo L (2018) Analytical bounds for the electromechanical buckling of a compressed nano-cantilever. Appl Math Model 59:571–582
25. Radi E, Bianchi G, Nobili A (2021) Bounds to the pull-in voltage of a MEMS/NEMS beam with surface elasticity. Appl Math Model 91:1211–1226
26. Bianchi G, Radi E (2020) Analytical estimates of the pull-in voltage for carbon nanotubes considering tip-charge concentration and intermolecular forces. Meccanica 55:193–209
27. Koochi A, Abadyan M (2020) Chapter 2 - Semianalytical solution methods. In: Koochi A, Abadyan M (eds) Nonlinear differential equations in micro/nano mechanics. Elsevier, Amsterdam
28. Dequesnes M, Tang Z, Aluru NR (2004) Static and dynamic analysis of carbon nanotube-based switches. J Eng Mater Technol Trans ASME 126:230–237
29. Hayt Jr WH, Buck JA, Akhtar MJ (2020) Engineering Electromagnetics| (SIE). McGraw-Hill Education
30. Israelachvili J (2011) Intermolecular and surface forces. Elsevier, Amsterdam
31. Timoshenko S, Woinowsky-Krieger S (1959) Theory of plates and shells. McGraw-Hill, New York
32. Sears A, Batra RC (2004) Macroscopic properties of carbon nanotubes from molecular-mechanics simulations. Phys Rev B - Condens Matter Mater Phys 69:1–10
33. Wolfram Research Inc. Mathematica 9.0
34. Zhang C, Xie S, Wang W, et al. Bio-syncretic tweezer: 3D manipulator actuated by microorganisms. In: 2015 IEEE International Conference on Robotics and Biomimetics, IEEE-ROBIO 2015 2015; 1979–1984
35. Sorrentino A, Bianchi G, Castagnetti D, et al. (2019) Experimental characterization of pull-in parameters for an electrostatically actuated cantilever. In: Proceedings of 30th International Conference on Adaptive Structures and Technologies, ICAST 2019 2019; 3: 69–70
36. Sanò P, Verotti M, Bosetti P et al (2018) Kinematic synthesis of a D-Drive MEMS device with rigid-body replacement method. J Mech Design Trans ASME 140:1–10
37. van West E, Yamamoto A, Higuchi T (2007) The concept of 'Haptic Tweezer', a non-contact object handling system using levitation techniques and haptics. Mechatronics 17:345–356
38. Sorrentino A, Bianchi G, Castagnetti D et al (2020) Experimental characterization of pull-in parameters for an electrostatically actuated cantilever. Appl Eng Sci 3:100014
39. Bitter R, Mohiuddin T, Nawrocki M (2017) LabVIEW™ Advanced Programming Techniques. CRC press
40. Rueden CT, Schindelin J, Hiner MC et al (2017) Image J2: IMAGEJ for the next generation of scientific image data. BMC Bioinformatics 18:1–26